Real-Time Synchrotron SAXS and WAXD Studies on Annealing Behavior of Poly[(*R*)-3-hydroxybutyrate] Single Crystals

Tomoharu Sawayanagi,[†] Toshihisa Tanaka,[‡] Tadahisa Iwata,[‡] Hideki Abe,[†,‡] Yoshiharu Doi,[†,‡] Kazuki Ito,[§] Tetsuro Fujisawa,[§] and Masahiro Fujita*[,‡]

Department of Innovative and Engineered Materials, Tokyo Institute of Technology, Nagatsuta 4259, Midori-ku, Yokohama 226-8502, Japan, Polymer Chemistry Laboratory, RIKEN Institute, Hirosawa 2-1, Wako-shi, Saitama 351-0198, Japan, and RIKEN Harima Institute/SPring-8, Kouto 1-1-1, Sayo-cho, Sayo-gun, Hyogo 679-5148, Japan

Received November 13, 2005; Revised Manuscript Received January 19, 2006

ABSTRACT: Poly[(*R*)-3-hydroxybutyrate] (P(3HB)) single crystals were grown isothermally at different crystallization temperatures (T_cs) in a dilute solution. Structural changes of the sedimented single-crystal mats on heating were followed by real-time synchrotron small-angle X-ray scattering (SAXS) and wide-angle X-ray diffraction (WAXD) techniques, and the dependence of the annealing behavior on T_c was examined. The two-dimensional (2D) SAXS pattern clearly demonstrated that the P(3HB) single crystal exhibits a discontinuous increase in the lamellar thickness at an annealing temperature. The onset of the discontinuous thickening depended on T_c or the initial lamellar thickness. The discontinuous thickening occurred at higher temperature as the initial lamellar thickness increased. In the transition region where the discontinuous thickening progressed, the new scattering peak intensity increased while the original one decreased. On the other hand, the crystallinity, estimated from the 2D WAXD patterns, first decreased and then recovered. The lamellar thickening was accompanied by endo- and exothermic signals in differential scanning calorimetry. Accordingly, the discontinuous lamellar thickening is caused by partial melting and recrystallization. The degree of recovery in crystallinity fell with increasing initial lamellar thickness. This is most probably because the crystallization rate becomes slower with increasing temperature in the transition region. After the transition, the long period between the reorganized lamellae increased, while the crystallinity decreased and, finally, diminished due to complete melting.

Introduction

Poly[(*R*)-3-hydroxybutyrate] (P(3HB)) is a biodegradable thermoplastic material, produced from renewable carbon sources by bacteria as intercellular carbon and energy reserves.[1,2] P(3HB) material has thus attracted much attention as an environmentally degradable material to be used for a wide range of agricultural, marine, and medical applications. From the enzymatic degradation experiments of the P(3HB) and its copolymers by some extracellular PHB depolymerases, it has been found that the degradation of material occurs first at amorphous regions and, subsequently, at the crystalline regions.[3,4] Accordingly, the crystalline regions in the material play an important role in the regulation of the biodegradability as well as the physical properties.[2] That is to say, revealing the detail of the crystalline structure is important to predict both the biodegradability and the physical properties of materials.

Solution-grown P(3HB) single crystal has been used as a model substrate to understand the correlation between crystalline structure and its biodegradability in the material.[5−11] It has been found that the biodegradability depends on the structural regularity in the crystal. To reveal the detail of the structural regularity and chain mobility in the crystal, annealing behavior of P(3HB) single crystals has been examined by X-ray technique and atomic force microscopy (AFM).[12−14] The X-ray studies on the annealing of P(3HB) single-crystal mats revealed that the annealed crystal exhibits a discontinuous increase in the long period at a certain temperature.[13] An in situ AFM annealing experiment of individual P(3HB) single crystal was also reported recently.[14] It was found that the single crystals drastically change above the annealing temperature due to melting, and the melting gradually proceeded from the lateral outer faces to the central portion. This behavior suggested that the chains at the lateral sides of the crystal have a higher level in mobility than those at the central portion of crystal.[14]

To follow in real time the fast dynamic changes such as phase transition in the annealing and melting processes of polymer crystals, the synchrotron X-ray technique is of greater advantage because the synchrotron small-angle X-ray scattering (SAXS) and wide-angle X-ray diffraction (WAXD) measurements can be made in a very short time frame and provide us fine details on the structural changes from the atomic scale up to macroscale events such as changes in lamellar morphology. In practice, the thermal behaviors of various polymer crystals, such as ultralong alkanes,[15−17] polyethylene (PE),[18,19] poly(aryl ether ketones),[20] syndiotactic polypropylene,[21] and oligo-3HB,[22,23] have been investigated by the synchrotron X-ray techniques. Many researchers have taken interest in the lamellar thickening during annealing or the chain mobility during the reorganization process. In low-molecular-weight polymers such as oligomer, the chains form lamellar crystals with a thickness that is an integer submultiple of the total chain length so that the drastic lamellar thickening due to chain unfolding occurs on heating.[15−17,23] This discontinuous nature of lamellar thickening is advantageous for better understanding the chain mobility during annealing. The ultralong alkanes crystals especially have been extensively studied as model systems of polymers using the synchrotron X-ray technique by Ungar and co-workers.[15,16] Recently, Terry et al. observed the annealing behavior of ultralong alkanes single

* To whom all correspondence should be addressed. E-mail: mfujita@riken.jp. Telephone: +81-48-467-9403. Fax: +81-48-462-4667.

[†] Department of Innovative and Engineered Materials, Tokyo Institute of Technology.

[‡] Polymer Chemistry Laboratory, RIKEN Institute.

[§] RIKEN Harima Institute/SPring-8.

10.1021/ma052425h CCC: $33.50
Published on Web 02/18/2006

crystals by using synchrotron WAXD.[17] They found that there is a reduction of the lattice parameters at an annealing temperature in the unfolding process. They associated the drop and recovery of the lattice parameters with partial melting (and recrystallization). Li et al. investigated the thickening process of oligo-3HB crystals on heating by synchrotron SAXS and WAXD.[23] They reported that the crystal also exhibits a discontinuous increase in thickness and the thickening process occurs via a partial melting and recrystallization. Such a discontinuous increase was also reported for higher-molecular-weight polymer crystals. The chain mobility in PE crystal during annealing was examined using synchrotron X-ray and Raman spectroscopy by Rastogi et al.[18] They found that a quantized thickening occurs even in the higher-molecular-weight polymer crystal on heating. They suggested that the quantized thickening of PE crystals is due to chain sliding diffusion, where the chains slide to the adjacent lamellar crystals along the chain axis.[18]

Our previous work revealed by real-time synchrotron X-ray technique that P(3HB) single crystals exhibit a similar discontinuous lamellar thickening on heating, although this is not the doubling of initial thickness.[24] The 2D SAXS pattern drastically changed at an annealing temperature where two different scattering peaks were observed, one is from the original lamellae and the other from the recrystallization lamellae. The structural changes observed by the SAXS and WAXD were in response to the thermal properties of the single crystals characterized by differential scanning calorimetry (DSC). These results indicated that the discontinuous lamellar thickening of P(3HB) single crystals is caused by partial melting and recrystallization.[24] In this paper, real-time annealing experiments for P(3HB) solution-grown single crystals that were prepared by different crystallization temperatures (T_c) were dealt with. The dependence of the annealing behavior on T_c was investigated by synchrotron SAXS and WAXD. In addition, thermal properties of the crystals were examined by DSC of the sedimented mat of single crystals. The results were compared with the structural evolution observed by SAXS and WAXD.

Experimental Section

Preparation of P(3HB) Single-Crystal Mats. Bacterial P(3HB) was supplied from Monsanto Co. The P(3HB) specimen used here was prepared by alkaline hydrolysis as follows:[7] P(3HB) (1 g) was dissolved in 120 mL of chloroform. After adding 40 mL of 1 N aqueous KOH and 800 mg of 18-crown-6 ether to the P(3HB) chloroform solution, the mixture was placed at 35 °C with stirring for 24 h. The organic layer was poured into methanol. The precipitated P(3HB) was obtained by vacuum filtration. The molecular weight was examined by gel permeation chromatography. The number-average molecular weight and polydispersity after the hydrolysis were 15 000 and 1.6, respectively. The P(3HB) single crystals were isothermally grown at T_c= 60, 80, and 100 °C for 24 h in 0.05 % w/v 1-octanol solution. The sedimented single-crystal mats were obtained by a filtration after the suspension was cooled to room temperature and then dried under vacuum.

Synchrotron SAXS and WAXD Measurements. Real-time SAXS and WAXD measurements were carried out at the BL45XU beam line (wavelength, $\lambda = 0.09$ nm) of the SPring-8, Harima, Japan. The camera lengths in the SAXS and WAXD measurements were about 2200 mm and 150 mm, respectively. A homemade sample-heating device was set in the beam line. The heating unit was controlled outside of the beam line station. The sample holder consists of two brass plates and is designed to sandwich a sample between their edges. The single-crystal mats were set in the sample holder and heated from room temperature to around 180 °C at a heating rate of 10 °C/min. All 2D SAXS and WAXD patterns were recorded with a CCD camera (C7300-10-12NR, Hamamatsu Photonics, Japan) coupled with an X-ray image intensifier (V5445P MOD, Hamamatsu Photonics, Japan). The pixel size of CCD camera was 125 μm × 125 μm. The exposure times in the SAXS and WAXD were determined in such a way that intensity signals were not saturated during the course of the experiment for any individual samples (22−1000 ms and 51−151 ms, respectively).

Data Analysis of SAXS and WAXD. The 2D SAXS images were converted to one-dimensional (1D) profiles according to the circular averaging method, as described in ref 25, by a Rigaku R-AXIS Display software package. Here, the averaging over the whole azimuthal angle was performed.[24] Subsequently, the Lorentz correction was applied to the integrated 1D profile after the subtraction of background. The individual scattering peak in the 1D profile was fitted by the Gaussian function with the IGOR Pro 4 software package. From the fitting parameters, the long period and the integral breadth of peak were estimated. The lattice dimensions (*a*-, *b*- and *c*-axes) and the apparent crystallite sizes (D_{200}, D_{020}, and D_{002}) were estimated from the peak positions and widths of 200, 020, and 002 reflections, respectively, in the equatorial and meridian line scans of 2D WAXD images. According to Scherrer's equation, the apparent crystallite sizes were calculated without any corrections, including deconvolution of instrumental broadening. For the estimation of crystallinity, the 2D WAXD images were converted to the integrated 1D profiles by the same procedure in SAXS analysis. Each of the crystalline peaks and amorphous scattering was fitted by the Gaussian function, and then the total area of crystalline peaks (A_c) and of the amorphous background (A_a) were calculated by the obtained fitting parameters. By using the A_c and the A_a, the crystallinity (X_c) was estimated.

Deferential Scanning Calorimetry. Thermal properties of P(3HB) single crystals were evaluated by DSC (Perkin-Elmer Pyris 1) of the sedimented single-crystal mats. The DSC thermograms were obtained under nitrogen atmosphere at a heating rate of 10 °C/min, which was the same rate as that in the synchrotron X-ray measurements.

Results

SAXS Measurements. Real-time SAXS measurements during annealing at 10 °C/min were performed for sedimented mats of solution-grown P(3HB) single crystals. The 2D SAXS patterns of P(3HB) single crystals, which were grown at T_c = 60, 80, and 100 °C, are shown in Figure 1. These patterns were taken at elevated temperatures (T_as). In Figure 1, the meridian is the lamellar stacking direction in the sedimented mats. The corresponding Lorentz-corrected 1D profiles are shown in Figure 2. The background increases upon decreasing angle in these figures. This is probably associated with voids between poorly stacked lamellar packets, as described in ref 16. The increments seem to depend on T_c. Hence, the reduction in orientation of crystal mats for higher T_c might be correlated with the formation of voids. The exact reason is, however, unclear at present.

The initial long periods estimated from the peak positions taken at room temperature were 4.0 nm ($q = 0.249$ nm^{-1}), 4.4 nm ($q = 0.228$ nm^{-1}), and 5.3 nm ($q = 0.189$ nm^{-1}) for T_c= 60, 80, and 100 °C, respectively (here, $q = 2 \sin \theta/\lambda$, 2θ: scattering angle). For solution-grown single-crystal mats, the long period can be regarded as one lamellar thickness. These values are certainly comparable with one lamellar thickness reported previously.[5−11,14] The original peak shifted little on heating to 120−130 °C. However, a new scattering peak at a lower angle was observed at a T_a for all single crystals, as indicated with the arrows in Figures 1 and 2. The new scattering peaks clearly recognized at $q = 0.155$ nm^{-1} at T_a = 122.5 °C for the crystal grown at T_c = 60 °C, $q = 0.154$ nm^{-1} at 127.5 °C for T_c = 80 °C, and $q = 0.154$ nm^{-1} at 132.5 °C for T_c = 100 °C, respectively. This fact means that the P(3HB) single crystal exhibits a discontinuous increase in lamellar thickness at the annealing temperature. The threshold temperature, at

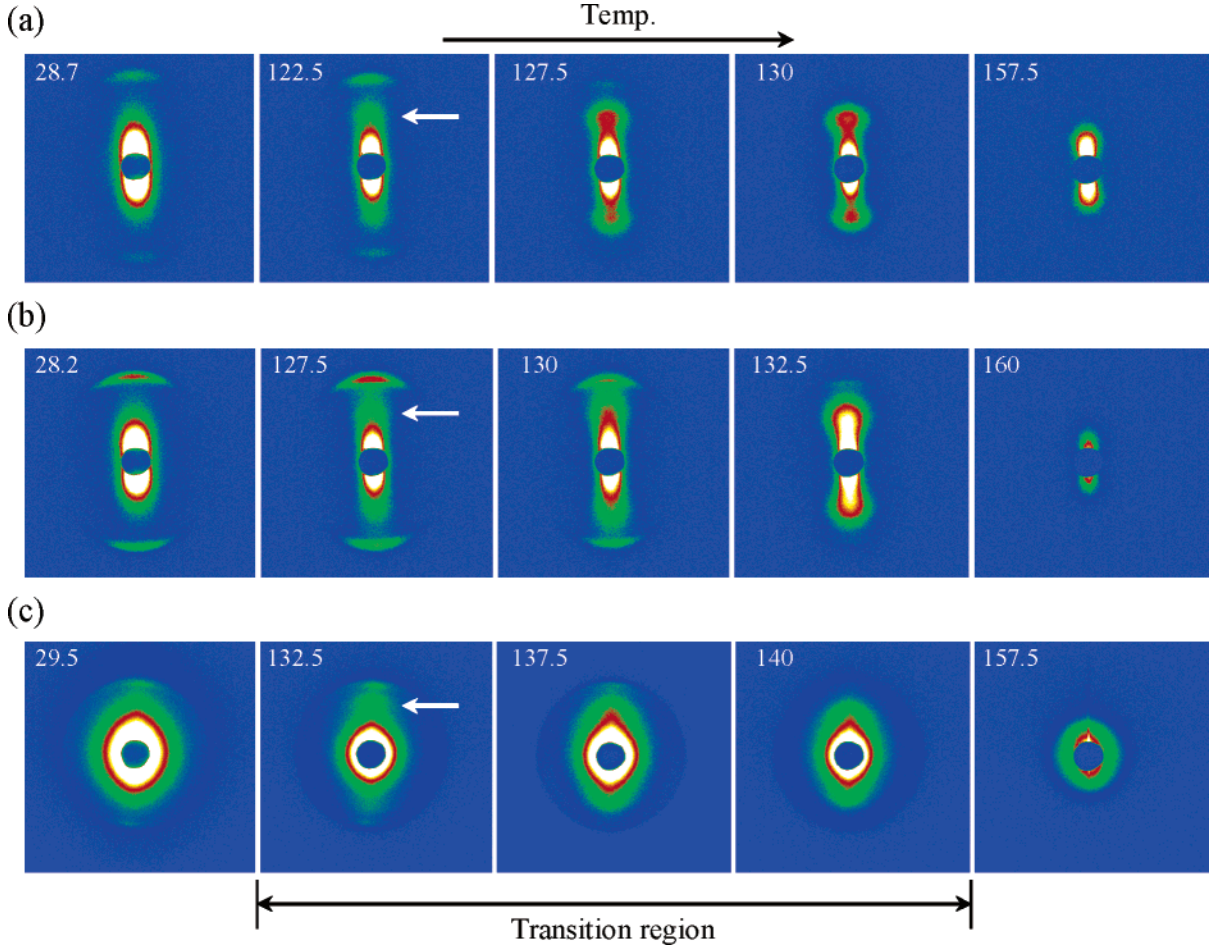

Figure 1. Two-dimensional SAXS patterns of sedimented mats of P(3HB) single crystals at elevated temperatures. These were taken at the temperatures indicated in the images. The series of (a), (b), and (c) represent the patterns of the single crystals grown at 60, 80, and 100 °C, respectively. In (a), (b), and (c), each arrow indicates a new scattering peak.

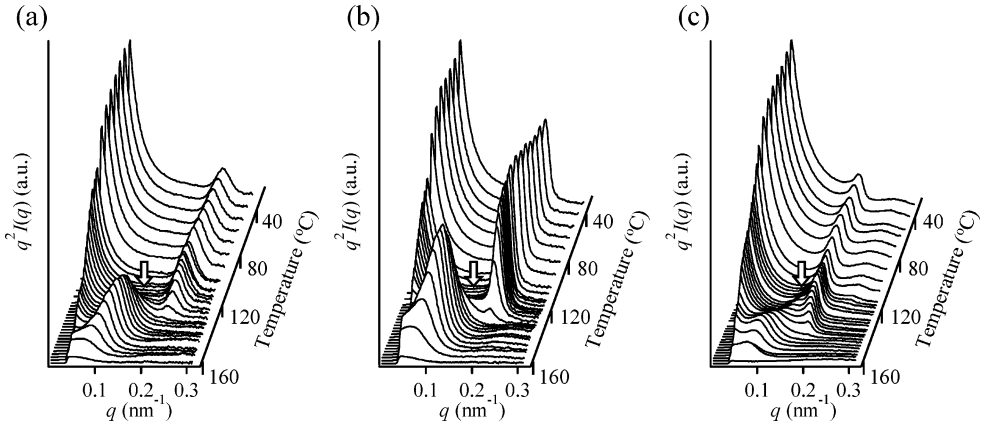

Figure 2. Lorentz-corrected 1D profiles derived from 2D SAXS patterns. The figures (a), (b), and (c) represent the profiles of the single crystals grown at 60, 80, and 100 °C, respectively. In (a), (b), and (c), each arrow indicates a new scattering peak.

which the discontinuous lamellar thickening starts, obviously depends on the T_c, that is, on the initial lamellar thickness. The new peak is attributed to the crystals reorganized from the original ones, as discussed later. Two crystal populations with different lamellar thicknesses could be detected up to $T_a = 130$, 132.5, and 140 °C for $T_c = 60$, 80, and 100 °C, respectively, as shown in Figures 1 and 2. After the complete transition of discontinuous increase, the remaining peak shifted to lower angle and, finally, diminished due to whole melting.

The lamellar thickness and the integral breadth of scattering peak against T_a are shown in Figure 3. These values were extracted from the integrated 1D SAXS profiles (Figure 2). As mentioned above, Figure 3 clearly demonstrates the discontinuous lamellar thickening and the coexistence of the two populations with different lamellar thicknesses. In the transition region, the original lamellar thickness slightly increased, suggesting that the thinner crystals in the original crystals reorganize in turn at lower T_a. On the other hand, the long period of reorganized crystal increased with increasing T_a, although a plateau region during the transition region was recognized in Figure 3a and b. The integral breadth of the new peak at the onset of discontinuous thickening was far broader than that of the original one

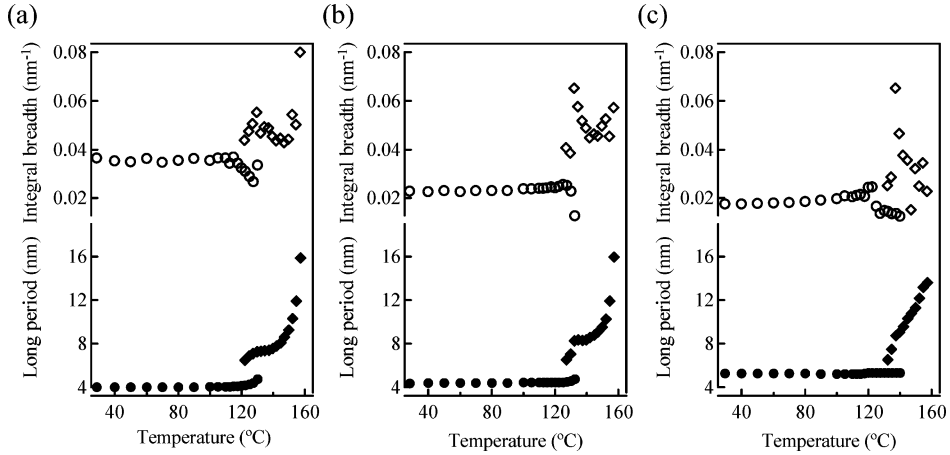

Figure 3. Temperature dependence of integral breadth (open symbol) and lamellar thickness (filled symbol) for P(3HB) single crystals grown at (a) 60, (b) 80, and (c) 100 °C. The circular and rhombic symbols indicate the original and reorganized crystals, respectively.

and became narrow during the lamellar thickening. It is indicated that the stacking of reorganized lamellae is less ordered at the initial stage and the structural order is improved by heating. Further annealing, the integral breadth increased again, associated with the reduction of structural order toward whole melting. These behaviors were independent of T_c.

In the oligomer crystals such as ultralong alkanes,[15−17] oligo-3HB,[22,23] and poly(ethylene oxide),[26] similar drastic change in lamellar thickness on heating has been reported previously. The drastic thickening during annealing is responsible for the unfolding of the integer folded form, and its process seems to be accompanied by partial melting and recrystallization.[23] In higher-molecular-weight polymer crystals, Rastogi et al. clearly demonstrated the doubling of lamellar thickness of PE crystals.[18] They also revealed that the crystals with two distinct thicknesses coexist during the lamellar thickening process, and the thickening is due to chain sliding diffusion along its axis.[18] Furthermore, similar behavior has been seen in polyamide single crystals.[27] To gain further insight into the mechanism of the discontinuous increase in lamellar thickness of P(3HB) single crystal, analyses of WAXD and DSC data are performed in this study.

WAXD and DSC Measurements. Real-time synchrotron WAXD measurements at a heating rate of 10 °C/min were performed for the sedimented mats of solution-grown P(3HB) single crystals grown at T_c = 60, 80, and 100 °C, respectively. The 2D WAXD patterns and the corresponding equatorial and meridional line scans on heating are shown in Figures 4 and 5. In Figure 4, the meridian is the lamellar stacking direction in the sedimented mats. Well-resolved fiber diffraction patterns of P(3HB) α-form[28] were obtained. As indexed in these figures, the 020, 110, and 200 reflections were recognized at about 2θ = 7.8°, 10.0°, and 16.7°, respectively, on the equatorial line (a*- and b*-axes), and the 002 reflection at about 2θ = 18.9° on the meridional line (c*-axis). The rightmost WAXD patterns in a series of images for each T_c were taken just before the complete melting, and the intensities in reflections were obviously reduced. To analyze the WAXD data more quantitatively, the annealing temperature dependence of the peak position and width were first investigated. Here, the temperature dependence of lattice dimensions (a-, b-, and c-axes) and apparent crystallite sizes (D_{200}, D_{020}, and D_{002}) were estimated from the peak positions and widths of 200, 020, and 002 reflections, respectively, in Figure 5. Figure 6 shows the temperature dependence of a-, b-, and c-axes. These dimensions in any T_a were calculated on the assumption that the unit cell is orthorhombic.[28] As reported in our previous work,[24] the thermal behavior of cell dimension is classified into three stages to demonstrate the relation between the morphological parameters obtained by SAXS, WAXD, and thermal properties, as shown below. In region I, the lattice dimensions increased gradually due to thermal expansion. It was found that the expansions continue up to around the onset of discontinuous increase in lamellar thickness. For a- and b-axes, these expansions seem to stop at the end of region I. In region II, that is, the transition region, the cell dimensions reduced. The contraction of the cell dimensions continued up to about 135, 140, and 150 °C for T_c = 60, 80, and 100 °C, respectively. Each of these temperatures is almost identical with the end of transition of the lamellar thickening (see Figures 1−3). The marked contraction of cell dimensions has been reported in the case of ultralong alkane crystal.[17] Furthermore, the contraction of the b-axis has been found in the oligo-3HB crystal in the unfolding process.[23] The molecular chains in the crystalline core are registered crystallographically so that the chain stems pack more rigidly than those near the fold surface. Accordingly, the increase in lamellar thickness or chain stem length will bring about the apparent contraction in the crystal lattice, as shown in Figure 6.[17] Finally, the all dimensions increased or remained almost constant in region III. In contrast to the cases of T_c = 60 (Figure 6a) and 80 °C (Figure 6b), for the single crystals grown at T_c = 100 °C, the cell dimensions, especially c-axis, did not exhibit definitive contraction in region II. This is probably because of the low intensity caused by the reduction in the orientation of the sample (see Figures 1c and 4c) brings about a lowering of precision to determine the peak position by curve fitting and/or the incomplete reorganization of the original crystal in this region. The reduction in orientation may be due to the existence of voids in the mat, as mentioned above.

Figure 7 shows the annealing temperature dependence of D_{200}, D_{020}, and D_{002}. This figure is also classified into the same three regions: all sizes remain almost constant in region I, increase in region II, and slightly increase or remain constant in region III. It is noteworthy that the D_{002} starts to increase from region II. This behavior is connected with the lamellar thickening observed by SAXS. Also, the D_{002} for T_c = 100 °C did not exhibit a definitive increase, in contrast to the case of T_c = 60 and 80 °C. This may be also due to the reduction in orientation of sample and/or incomplete reorganization of crystals.

Next, the annealing temperature dependence of crystallinity was examined, in addition to DSC analysis. The change in X_c and the DSC curve with temperature is shown in Figure 8. Here, the X_c is the relative value when the crystallinity at room

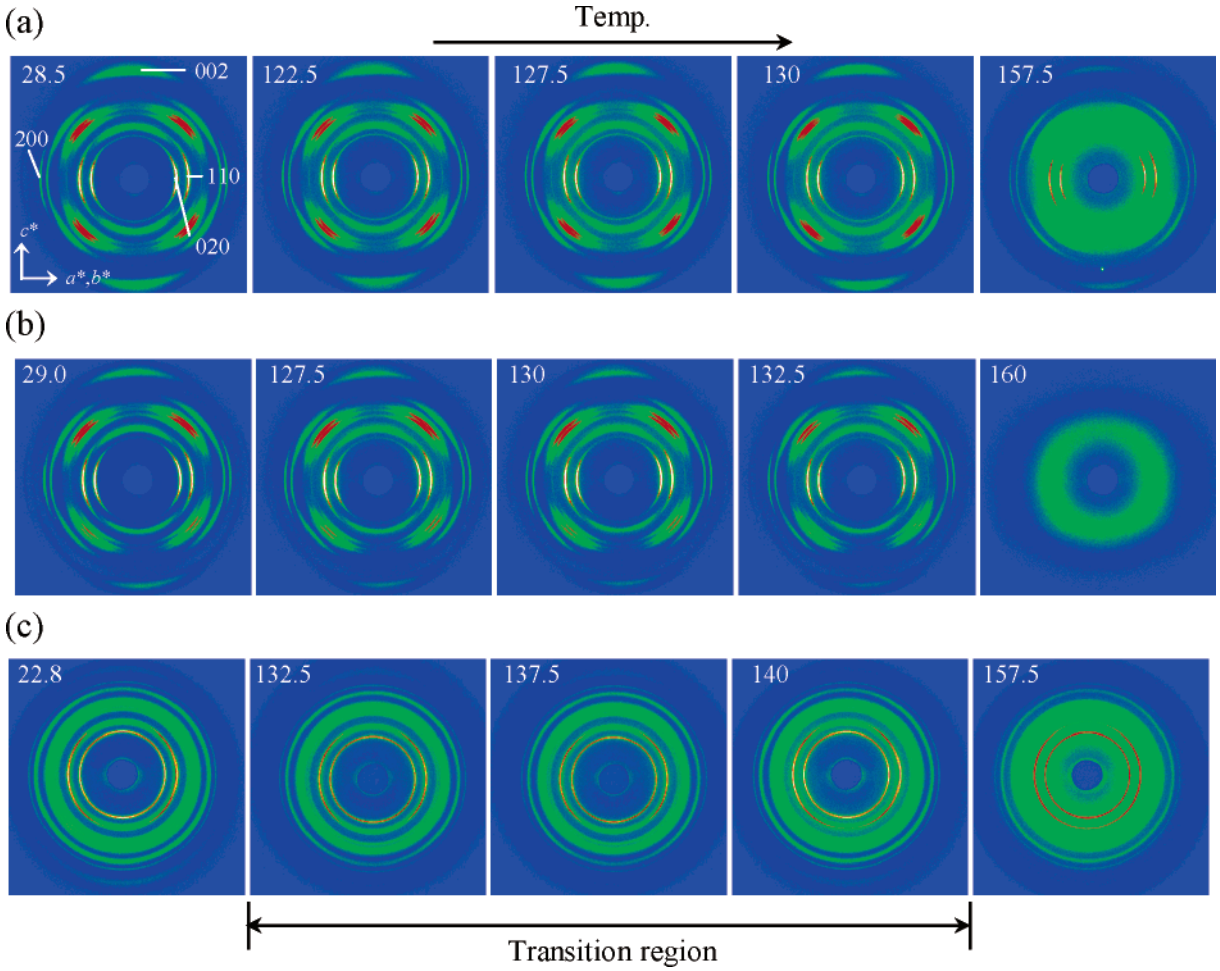

Figure 4. Two-dimensional WAXD patterns of sedimented mats of P(3HB) single crystals at elevated temperatures, which were taken at the temperatures indicated in the images. The series of (a), (b), and (c) represent the patterns of the single crystals grown at 60, 80, and 100 °C, respectively.

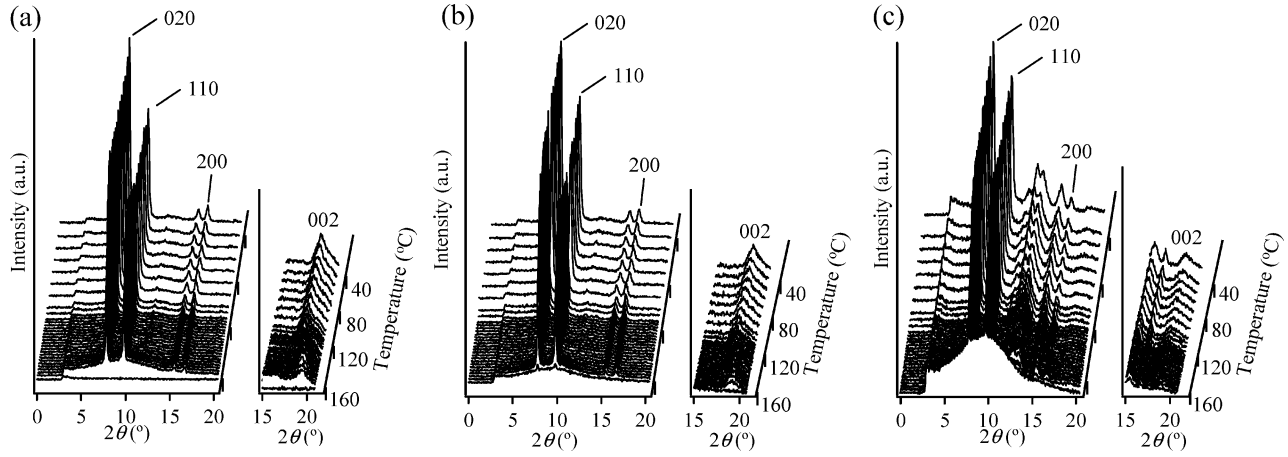

Figure 5. Equatorial and meridional line scans of WAXD patterns with representative crystalline reflection indices for the single crystals grown at (a) 60, (b) 80, and (c) 100 °C, respectively.

temperature is 1.0. In the DSC curve, the trace below 120 °C is not due to the structural change of the sample but due to the curvature of baseline. As can be seen in Figure 8, the classification into three regions is in response to the heat evolution of the DSC curve: region I is up to the onset of lower endothermic signal, region II from there to the exothermic peak, and region III corresponds to the higher endothermic signal. Independent of T_c, the X_cs remained unchanged in region I. Thereafter, the X_cs showed a tendency to first decrease, and then recover, in region II. However, these trends were dependent on the T_c of each sample. The decrease in X_c occurs in the range of the lower endotherm, suggesting that the original crystals melt. The next recovery is associated with recrystallization because the maximum or shoulder in X_c exhibited at 135, 142.5, and 152.5 °C for T_c = 60, 80, and 100 °C, respectively, is almost consistent with the temperature that reaches a minimum (136.5, 138.8, and 148.2 °C for T_c = 60, 80, and 100 °C, respectively, see Table 1) in the corresponding DSC curve. As shown in Figure 8c, the X_c for T_c = 100 °C did not recover completely. The original crystals grown at higher temperature start their

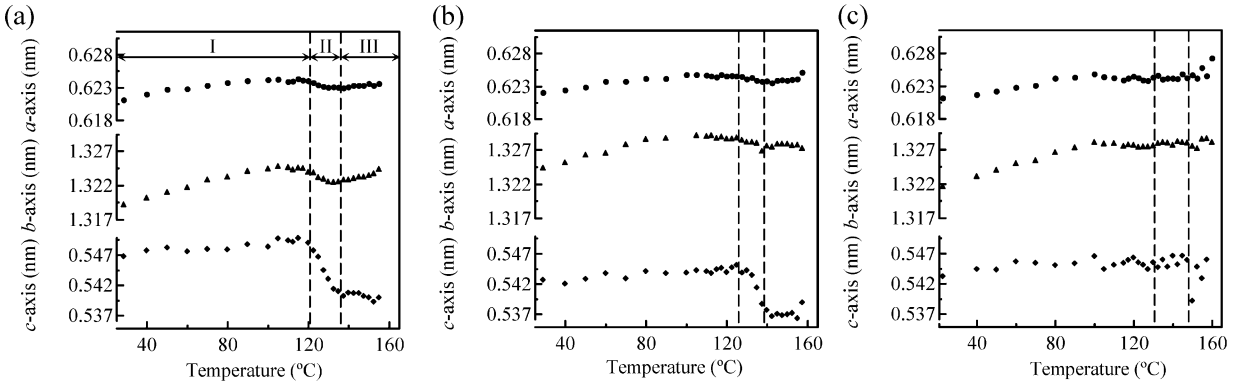

Figure 6. Lattice dimensions as a function of temperature for P(3HB) single crystals grown at (a) 60, (b) 80, and (c) 100 °C, respectively.

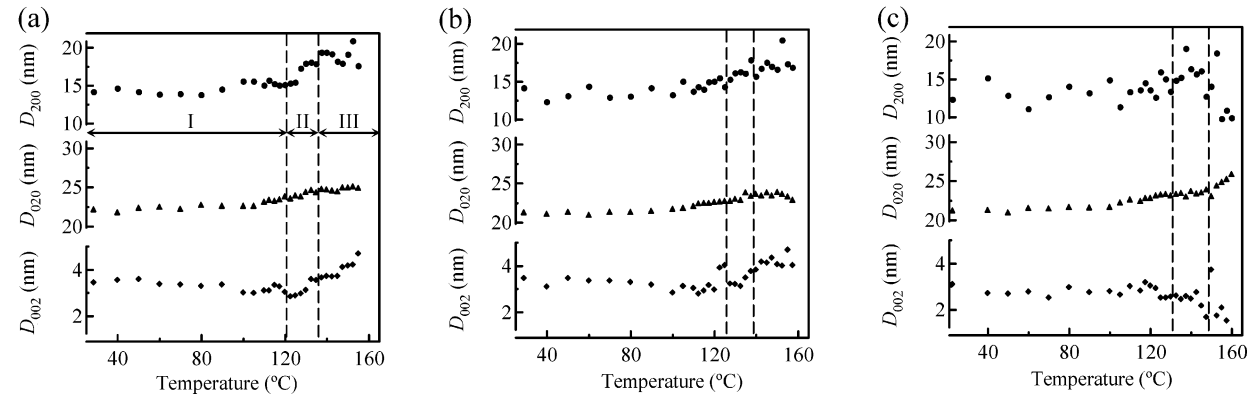

Figure 7. Apparent crystallite sizes as a function of temperature for P(3HB) single crystals grown at (a) 60, (b) 80, and (c) 100 °C, respectively.

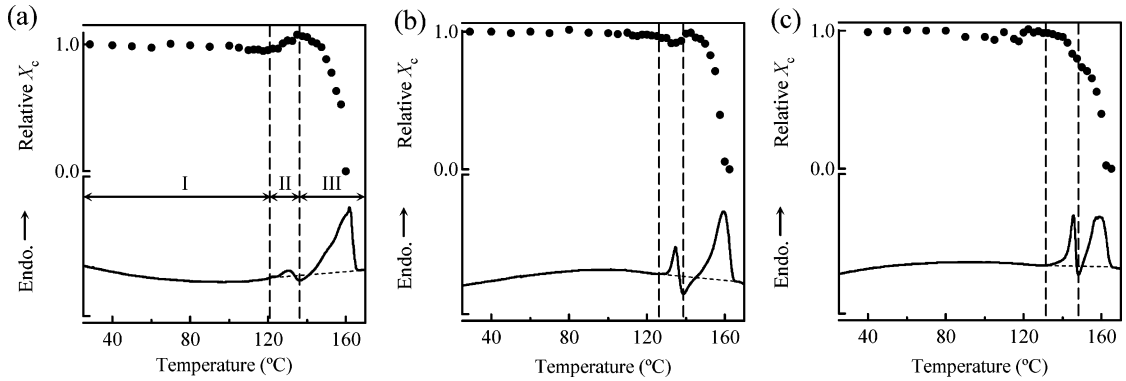

Figure 8. Relative crystallinities estimated from 2D WAXD as a function of temperature and DSC curves for P(3HB) single crystals grown at (a) 60, (b) 80, and (c) 100 °C, respectively.

Table 1. Thermal Properties of P(3HB) Single Crystal Mats

T_c, °C	T_{Lm},[a] °C	ΔH_{Lm},[b] J/g	T_{rc},[c] °C	ΔH_{rc},[d] J/g	T_{Hm},[e] °C	ΔH_{Hm},[f] J/g
60	130.9	3.70	136.5	1.62	160.2	55.98
80	134.5	7.90	138.8	7.28	159.5	52.87
100	145.6	20.82	148.2	1.09	158.9	47.32

[a] T_{Lm}: lower endotherm peak (lower melting temperature). [b] ΔH_{Lm}: enthalpy of fusion per gram of polymer calculated from lower endotherm peak. [c] T_{rc}: exotherm peak (recrystallization temperature). [d] ΔH_{rc}: enthalpy of recrystallization per gram of polymer calculated from exotherm peak. [e] T_{Hm}: higher endotherm peak (higher melting temperature). [f] ΔH_{Hm}: enthalpy of fusion per gram of polymer calculated from higher endotherm peak.

discontinuous lamellar thickening, or partial melting, at higher T_a. This leads to the recrystallization at a higher temperature. In the temperature range of the thickening process, the crystallization rate becomes probably slower with increasing temperature.[29] Accordingly, the thicker crystals cannot transform sufficiently into newly reorganized ones by the partial melting and recrystallization, especially for the case of $T_c = 100$ °C, as shown in Figure 8c. In region III, the X_cs dropped to zero. This is evidently associated with complete melting of the reorganized crystals.

The structural changes can also be explained in terms of thermal properties characterized by DSC. Table 1 is the summary of the thermal properties for the single-crystal mats used here. The apparent enthalpies of fusion for the lower and higher melting (ΔH_{Lm}, ΔH_{Hm}) and enthalpy of recrystallization (ΔH_{rc}) were determined from the peak areas above and below a linear baseline, respectively, as illustrated in Figure 8. The magnitude of ΔH_{Lm} and ΔH_{rc} will be caused by the balance between melting and recrystallization of the polymer. The lamellar thickening of thinner crystals accompanies faster recrystallization just after the crystals melt, so that the resulting ΔH_{Lm} will decrease with decreasing in T_c, and ΔH_{rc} will thus decrease with decreasing in T_c. However, the ΔH_{rc} for $T_c = 100$ °C was smaller than that for $T_c = 80$ °C. This is because

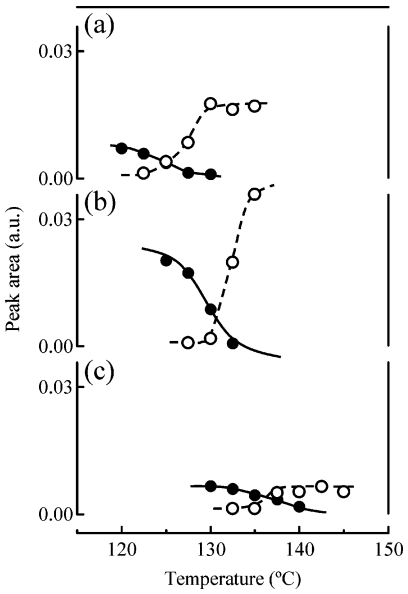

Figure 9. SAXS peak area from original crystal (filled symbol) and reorganized crystal (open symbol) against annealing temperature during discontinuous thickening. The figures (a), (b), and (c) correspond to the P(3HB) single crystals grown at 60, 80, and 100 °C, respectively.

that the molten chains do not recrystallize sufficiently during the thickening process due to slow crystallization at the high temperature. This is consistent with the change in X_c. The ΔH_{Hm} is associated with complete melting of recrystallized lamellae. This is supported by the fact that there is little difference between the ΔH_{Hm}s for $T_c = 60$ and 80 °C. The ΔH_{Hm} of the crystals grown at $T_c = 100$ °C was smaller than those of the crystals at $T_c = 60$ and 80 °C. This is because the X_c for $T_c = 100$ °C recovered up to only 75−80%, as shown in Figure 8.

Discussion

The present real-time synchrotron SAXS and WAXD measurements of P(3HB) single crystals during annealing have revealed that the P(3HB) single crystal exhibits a unique annealing behavior. The onset of the discontinuous lamellar thickening depended on T_c, that is, on the initial lamellar thickness. This is probably because the motion of chains is more limited as the initial lamellar thickness increases. The cell dimensions exhibit maxima near the boundary between regions I and II, indicating that the maxima corresponded to a unit cell size in which restrictions on chain movement are released. Interestingly, the change of the *c*-axis lagged behind those of the *a*- and *b*-axes (Figure 6). There is a possibility that the *a*- and *b*-axes exhibit apparent maxima at lower annealing temperatures because the crystal structure may deviate from the orthorhombic unit cell,[28] e.g., by lattice skew.[23] The behavior of the *c*-axis rather than those of the *a*- and *b*-axes, however, corresponded more strictly to the lamellar thickening process. It is hence deduced that the thermal energy may be first transformed into chain rotation or conformational disordering and then into chain translation.[30] At that time, the original crystals started to transform into a more stable state, that is to say, the lamellar thickening started (Figure 3). The crystallinity first decreased and then recovered. For the heat evolution accompanied by the structural transition, endotherm and subsequent exotherm-like signals were observed in the DSC measurement in region II (Figure 8). It is evident that the discontinuous increase in thickness for P(3HB) single crystal is due to partial melting and subsequent recrystallization. Figure 9 shows the plot of the SAXS peak area against T_a during discontinuous thickening. In this figure, the filled and open symbols indicate the areas of scattering peaks from the original and reorganized crystals, respectively. As can be seen in Figure 9, the population of reorganized crystals increases, while that of the original ones decrease with temperature, suggesting that the reorganized crystals are from the original crystals and all crystals do not thicken simultaneously. In addition, even if one lamellar crystal has a uniform thickness, the discontinuous thickening starts in the order of less thermally stable crystallites with a smaller size or defect in the crystal. This is supported by the experimental evidence that apparent crystallite sizes increase gradually (Figure 7). The recent AFM studies on thermal behavior of polymer single crystals have also revealed visually that local reorganization within the crystal precedes during annealing.[14,31−38] In this way, the discontinuous lamellar thickening progresses, and as a result, the population of newly reorganized crystals increases gradually with temperature.

As reported by recent in situ AFM annealing experiments, the molecular mechanism in thickening of an isolated single crystal has been gradually clarified.[14,31−38] In a sedimented mat of solution-grown single crystals, the crystals are regularly stacked along the chain direction in contrast to the isolated crystal, and furthermore, there is not an amorphous layer between the crystals in contrast to the bulk materials. If only one crystal begins to thicken by heating, the thickening is probably prevented by the adjacent crystals. Hence, the discontinuous lamellar thickening of the crystal will be a cooperative process, with the adjacent ones along the stacking direction. This is supported by the fact that the stacking direction of lamellar crystals or the chain axis direction is maintained before and after reorganization, as revealed by the present 2D SAXS and WAXD patterns. The chains, thus, mutually diffuse, leading to a thicker crystal in the space in which the adjacent crystal existed, similar to the models proposed previously by Rastogi et al.,[18] Statton,[39] and Dreyfuss et al.[40] One of them is the solid-state reorganization process that the chains slide along the crystal lattice,[18,40] and the other the melting−recrystallization process.[39] In the present case, we have considered that the thickening of P(3HB) crystals proceeds via partial melting and subsequent recrystallization. Interestingly, the long period of the reorganized crystals at the initial stage of discontinuous thickening was almost independent of T_c, as shown in Figure 3. It is deduced that the chain rearrangement in the thickening is interfered with by the surrounding crystals that are newly reorganized and/or perhaps still unthickened.

After the transition, the crystallinity showed decrease to zero. This result indicates that an amorphous region increases consecutively. In this high T_a region, the increase in the D_{002} was small (Figure 7). Thus, the increase in the long period in region III will be mainly associated with the increase in the interlamellar distance by melting of adjacent thinner lamellae rather than the increase in lamellar thickness of the individual crystal.[20,41] This will occur randomly in the mat and, as a result, causes the final broadening of the SAXS peak (Figure 3).

Concluding Remarks

P(3HB) single crystals were grown isothermally at different T_cs in a dilute 1-octanol solution. Fast structural changes of the sedimented single-crystal mats on heating could be followed by real-time synchrotron SAXS and WAXD techniques, and the dependence of the annealing behavior on T_c was examined. The 2D SAXS pattern of single-crystal mats drastically changed at a T_a, where a new scattering peak was recognized at lower angle together with the original peak. It was demonstrated that

the P(3HB) single crystal exhibits a discontinuous increase in lamellar thickness. The onset of the discontinuous lamellar thickening depended on T_c, that is, the initial lamellar thickness. The discontinuous thickening occurred at a higher temperature as the initial lamellar thickness increased. In the transition region where the discontinuous lamellar thickening progressed, the new scattering peak intensity increased, while the original one decreased. The transition was observed over a wide range of temperature. After the transition, the new scattering peak shifted to lower angle and, finally, diminished due to complete melting. The changes in lattice dimension, crystallite size, and crystallinity during annealing were also estimated from the 2D WAXD patterns. During the thickening process, the crystallinity first decreased and then recovered. The degree of recovery in crystallinity fell with increasing in the initial lamellar thickness. This is most probably because the crystallization rate becomes slower with an increase in temperature in the transition region. In addition, the lamellar thickening was accompanied by endo- and exothermic signals in DSC. Accordingly, the discontinuous lamellar thickening of P(3HB) single crystals is caused by partial melting and recrystallization. We have considered that the discontinuous lamellar thickening will be a cooperative process with the adjacent ones along the stacking direction. The chains mutually diffuse, leading to a thicker crystal, into the space in which the adjacent crystal existed. After the transition, the long period between the reorganized lamellae increased, while the crystallinity decreased and, finally, diminished due to complete melting.

Acknowledgment. This work has been partly supported by grants of Ecomolecular Science Research from RIKEN Institute, SORST of Japan Science and Technology Agency (JST), by a DRI Director's Grant from RIKEN Institute (to M.F.), and a Grant-in-Aid for Young Scientists (A) from the Ministry of Education, Culture, Sports, Science, and Technology of Japan (no. 15685009) (to T.I.). We also thank Yamamoto-Seisakujo, Japan, and KEYENCE Co., Ltd., for making the sample heat device and its remote control unit, respectively.

References and Notes

(1) Doi, Y. *Microbial Polyesters*; VCH: New York, 1990.
(2) Sudesh, K.; Abe, H.; Doi, Y. *Prog. Polym. Sci.* **2000**, *25*, 1503−1555.
(3) Tomasi, G.; Scandola, M.; Briese, B. H.; Jendrossek, D. *Macromolecules* **1996**, *29*, 507−513.
(4) Abe, H.; Doi, Y.; Aoki, H.; Akehata, T. *Macromolcules* **1998**, *31*, 1791−1797.
(5) Hocking, P. J.; Marchessault, R. H.; Timmins, M. R.; Lentz, R. W.; Fuller, R. C. *Macromolecules* **1996**, *29*, 2472−2478.
(6) Nobes, G. A. R.; Marchessault, R. H.; Chanzy, H.; Bries, B. H.; Jendrossek, D. *Macromolecules* **1996**, *29*, 8330−8333.
(7) Iwata, T.; Doi, Y.; Kasuya, K.; Inoue, Y. *Macromolecules* **1997**, *30*, 833−839.
(8) Iwata, T.; Doi, Y.; Tanaka, T.; Akehata, T.; Shiromo, M.; Teramachi, S. *Macromolecules* **1997**, *30*, 5290−5296.
(9) Iwata, T.; Doi, Y. *Macromol. Chem. Phys.* **1999**, *200*, 2429−2442.
(10) Iwata, T.; Doi, Y.; Kokubu, F.; Teramachi, S. *Macromolcules* **1999**, *32*, 8325−8330.
(11) Murase, T.; Iwata, T.; Doi, Y. *Macromolecules* **2001**, *34*, 5848−5853.
(12) Marchessault, R. H.; Coulombe, S.; Morikawa, H.; Okamura, K.; Revol, J. F. *Can. J. Chem.* **1981**, *59*, 38−44.
(13) Mitomo, H.; Doi, Y. *Int. J. Biol. Macromol.* **1999**, *25*, 201−205.
(14) Fujita, M.; Iwata, T.; Doi, Y. *Polym. Degrad. Stab.* **2003**, *81*, 131−139.
(15) Ungar, G.; Zeng, X. *Chem. Rev.* **2001**, *101*, 4157−4188.
(16) de Silva, D. S. M.; Zeng, X.; Ungar, G., Spells, S. J. *Macromolecules* **2002**, *35*, 7730−7741.
(17) Terry, A. E.; Phillips, T. L.; Hobbs, J. K. *Macromolecules* **2003**, *36*, 3240−3244.
(18) Rastogi, S.; Spoelstra, A. B.; Goossens, J. G. P.; Lemstra, P. J. *Macromolecules* **1997**, *30*, 7880−7889.
(19) Rastogi, S.; Kurelec, L.; Lemstra, P. J. *Macromolecules* **1998**, *31*, 5022−5031.
(20) Krüger, K. N.; Zachmann, H. G. *Macromolecules* **1993**, *26*, 5202−5208.
(21) Wang, Z. G.; Wang, X. H.; Hsiao, B. S.; Phillips, R. A.; Medellin-Rodriguez, F. J.; Srinivas, S.; Wang, H.; Han, C. C. *J. Polym. Sci., Part B: Polym. Phys.* **2001**, *39*, 2982−2995.
(22) Organ, S. J.; Li, J.; Terry, A. E.; Hobbs, J. K.; Barham, P. J. *Polymer* **2004**, *45*, 8925−8936.
(23) Li, J.; Organ, S. J.; Terry, A. E.; Hobbs, J. K.; Barham, P. J. *Polymer* **2004**, *45*, 8937−8947.
(24) Fujita, M.; Sawayanagi, T.; Tanaka, T.; Iwata, T.; Abe, H.; Doi, Y.; Ito, K.; Fujisawa, T. *Macromol. Rapid Commun.* **2005**, *26*, 678−683.
(25) Kumaraswamy, G.; Verma, R. K.; Kornfield, J. A.; Yeh, F.; Hsiao, B. S. *Macromolecules* **2004**, *37*, 9005−9017.
(26) Kovacs, A. J.; Straupe, C. *Faraday Discuss. Chem. Soc.* **1979**, *68*, 225−238.
(27) Dreyfuss, P.; Keller, A. *J. Macromol. Sci., Phys. B* **1970**, *4*, 811−836.
(28) Yokouchi, M.; Chatani, Y.; Tadokoro, H.; Teranishi, K.; Tani, H. *Polymer* **1973**, *14*, 267−272.
(29) Abe, H.; Doi, Y. *Biomacromolecules* **2002**, *3*, 133−138.
(30) Mansfield, M.; Boyd, R. H. *J. Polym. Sci., Polym. Phys. Ed.* **1978**, *16*, 1227−1252.
(31) Winkel, A. K.; Hobbs, J. K.; Miles, M. J. *Polymer* **2000**, *41*, 8791−8800.
(32) Tian, M.; Loos, J. *J. Polym. Sci., Part B: Polym. Phys.* **2001**, *39*, 763−770.
(33) Magonov, S. N.; Yerina, N. A.; Ungar, G.; Reneker, D. H.; Ivanov, D. A. *Macromolecules* **2003**, *36*, 5637−5649.
(34) Fujita, M.; Doi, Y. *Biomacromolecules* **2003**, *4*, 1301−1307.
(35) Nakamura, J.; Kawaguchi, A. *Macromolecules* **2004**, *37*, 3725−3734.
(36) Organ, S. J.; Hobbs, J. K.; Miles, M. J. *Macromolecules* **2004**, *37*, 4562−4572.
(37) Sanz, N.; Hobbs, J. K.; Miles, M. J. *Langmuir* **2004**, *20*, 5989−5997.
(38) Zhai, X.-M.; Wang, W.; Ma, Z.-P.; Wen, X.-J.; Yuan, F.; Tang, X.-F.; He, B.-L. *Macromolecules* **2005**, *38*, 1717−1722.
(39) Statton, W. O. *J. Appl. Phys.* **1967**, *38*, 4149−4151.
(40) Dreyfuss, P.; Keller, A. *J. Polym. Sci., Polym. Lett. Ed.* **1970**, *8*, 253−258.
(41) Cho, M. H.; Kyu, T.; Lin, J. S.; Saijo, K.; Hashimoto, T. *Polymer* **1992**, *33*, 4152−4157.

MA052425H